CHANDRA OBSERVATIONS OF MBM 12 AND MODELS OF THE LOCAL BUBBLE

R. K. SMITH

NASA Goddard Space Flight Center, Code 662, Greenbelt, MD 20771; and Department of Physics and Astronomy,
The Johns Hopkins University, 3400 North Charles Street, Baltimore, MD 21218; rsmith@milkyway.gsfc.nasa.gov

R. J. EDGAR, P. P. PLUCINSKY, AND B. J. WARGELIN

Harvard-Smithsonian Center for Astrophysics, 60 Garden Street, Cambridge, MA 02138

P. E. FREEMAN

Department of Statistics, Carnegie Mellon University, 5000 Forbes Avenue, Pittsburgh, PA 15213

AND

B. A. BILLER

Steward Observatory, University of Arizona, 933 North Cherry Avenue, Tucson, AZ 85721

Received 2004 September 24; accepted 2005 January 3

ABSTRACT

Chandra observations toward the nearby molecular cloud MBM 12 show unexpectedly strong and nearly equal foreground O VIII and O VII emission. As the observed portion of MBM 12 is optically thick at these energies, the emission lines must be formed nearby, coming from either the Local Bubble (LB) or charge exchange with ions from the Sun. Equilibrium models for the LB predict stronger O VII than O VIII, so these results suggest that the LB is far from equilibrium or that a substantial portion of O VIII is from another source, such as charge exchange within the solar system. Despite the likely contamination, we can combine our results with other EUV and X-ray observations to reject LB models that posit a cool recombining plasma as the source of LB X-rays.

Subject headings: ISM: bubbles — plasmas — supernova remnants — X-rays: ISM

Online material: color figure

1. INTRODUCTION

After decades of observation, the nature of the diffuse soft ($\sim\frac{1}{4}$ keV) X-ray background is still mysterious. Early observations of soft X-ray emission toward many sight lines (Bowyer et al. 1968; Bunner et al. 1969; Davidsen et al. 1972) showed that there is substantial diffuse emission (see also reviews by Tanaka & Bleeker 1977; McCammon & Sanders 1990). Broadband spectral data from proportional counter observations fit a three-component model: an unabsorbed 10^6 K thermal component, an absorbed 2×10^6 K thermal component, and an absorbed power law. The latter two components contribute mostly at higher energies, while most of the $\frac{1}{4}$ keV band comes from the local (i.e., unabsorbed) 10^6 K thermal component.

Williamson et al. (1974) excluded on physical grounds all then-proposed sources for the $\frac{1}{4}$ keV band emission other than a hot ($\sim10^6$ K) ionized plasma. Current theories to explain the origin of this emission still require an ionized plasma, and include (1) a local young supernova explosion in a cavity (Cox & Anderson 1982; Edgar & Cox 1993), (2) a series of supernovae (Innes & Hartquist 1984; Smith & Cox 2001), or (3) an over-ionized plasma slowly recombining after substantial adiabatic cooling (Breitschwerdt & Schmutzler 1994; Frisch 1995; Breitschwerdt et al. 1996). One additional possibility was first suggested by Cox (1998), who pointed out that charge exchange from the solar wind might create at least part of the $\frac{1}{4}$ keV band emission.

Independent of the observed $\frac{1}{4}$ keV band emission, absorption-line measurements to many nearby stars (e.g., Welsh et al. 1990, 1991) show that we are surrounded by a irregularly shaped "cavity" with very low density. The standard model for the Local Bubble (LB) combines these two observations into the "displacement" model (Sanders et al. 1977; Snowden et al. 1990). In this picture, the diffuse X-rays come from an elongated bubble of hot gas with average radius $\sim$100 pc, with the Sun near the center. If the LB is filled with hot ($\sim10^6$ K) gas in collisional ionization equilibrium (CIE), then the models of the resulting emission fit the observed $\frac{1}{4}$ keV band soft X-ray spectrum. However, this phenomenological model explains neither the origin of the hot gas nor the low-density region.

Early LB models that attempted to explain both the hot gas and the low-density region (Cox & Anderson 1982; Edgar & Cox 1993) modeled it as an $\sim10^5$ yr old supernova remnant. However, this model predicts a large column density of O VI that is simply not observed along many sight lines (Shelton & Cox 1994; Oegerle et al. 2005). Since every oxygen atom passing through the blast wave needs to pass through this ionization state, the model predictions are quite robust and are simply not observed. In addition, the total thermal energy required by the phenomenological models is between 0.37×10^{51} and 1.1×10^{51} ergs—nearly the entire kinetic energy of a supernova. Smith & Cox (2001) considered models with multiple supernovae that are allowed by the O VI data and energy considerations and that roughly fit the observed broadband emission. The recombining plasma model, described in detail in Breitschwerdt et al. (1996), has also been able to qualitatively fit existing observations. However, as discussed below, we are now able to reject the basic recombining plasma model by combining our results with other EUV and X-ray observations.

2. X-RAY EMISSION FROM THE LOCAL BUBBLE

The difficulty in measuring the soft X-ray spectrum has limited further analysis. A 10^6 K plasma with solar abundances, in equilibrium or not, is line dominated in the range $0.1-1.0$ keV, but the first observation able to even partially resolve these lines was done only recently with the Diffuse X-Ray Spectrometer

(DXS; Sanders et al. 2001). Most of the lines are from L-shell ions of elements from the third row of the periodic chart: Si, S, Mg (and their neighbor Ne), and M-shell ions of Fe around 72 eV. There should also be some X-ray emission from the K-shell lines of carbon, nitrogen, and oxygen.

Fitting the spectrum requires a spectral emission code for a collisional plasma, such as described in Smith et al. (2001) or Kaastra & Jansen (1993). These codes model the thousands of lines emitted by the cosmically abundant elements because of collisional excitation. However, the lines in the observed spectrum are numerous, and the atomic data for the line emission are incomplete and sometimes inaccurate. In any event, no calculated spectrum matches the high-resolution observations of the soft X-ray spectrum, such as those from DXS, and it is not clear whether the problem lies in the physical models or in the atomic data (Sanders et al. 2001). To avoid these problems, unambiguous and strong emission lines are needed. In a 10^6 K plasma, the most abundant line-emitting element is oxygen. In equilibrium at 10^6 K the dominant stage is helium-like O^{+6}, with trace amounts of O^{+7} and O^{+5}. However, the hot gas in the LB need not be in equilibrium. If (somehow) a recent ($\lesssim 10^5$ yr) supernova created the LB, then the gas would still be ionizing. Conversely, if the LB is old ($\gtrsim 10^6$ yr), then it should be recombining. In either case, the ratios of the O^{+6} and O^{+7} ion populations will not be at their equilibrium values.

The strongest O VII and O VIII emission lines are in the soft X-ray range, between 0.5 and 0.8 keV. O VII has a triplet of lines from $n = 2 \rightarrow 1$, the so-called forbidden (F) line at 0.561 keV, the resonance (R) line at 0.574 keV, and the intercombination (I) line (actually two lines) at 0.569 keV, while O VIII has a Lyα transition at 0.654 keV. These lines are regularly used as plasma diagnostics in other situations: Acton & Brown (1978) discussed the nonequilibrium ionization effects on O VII lines in solar flares. Vedder et al. (1986), using data from the *Einstein* Focal Plane Crystal Spectrometer (FPCS), measured the ionization state in the Cygnus Loop using these lines. Gabriel et al. (1991) discussed the general use of O VII and O VIII emission lines in hot plasmas, specifically applied to *Einstein* FPCS observations of the Puppis remnant. The goal of our work is to apply these methods, already used to model supernova remnants, to the specific case of the LB.

Earlier observations suggested that oxygen emission lines are strong in the LB. Inoue et al. (1979) detected the O VII F+ I+R emission lines with a gas scintillation proportional counter. Schnopper et al. (1982) and Rocchia et al. (1984), using solid-state Si(Li) detectors, detected O VII as well as lines from other ions. More recently, a sounding rocket flight of the X-Ray Quantum Calorimeter (XQC) observed a 1 sr region of the sky at high Galactic latitude between 0.1 and 1 keV with an energy resolution of 5–12 eV, and detected both O VII and O VIII. The O VII flux was 4.8 ± 0.8 photons cm^{-2} s^{-1} sr^{-1} (hereafter line units, LU), and the O VIII flux was 1.6 ± 0.4 LU (McCammon et al. 2002). XQC's large field of view means that the source of the photons cannot be determined, but this does represent a useful upper limit to the LB emission in this direction.

Measuring the emission coming solely from the LB requires observations of clouds that shadow the external emission. Snowden et al. (1993, hereafter SMV93) used *ROSAT* observations of the cloud MBM 12 to measure the $\frac{3}{4}$ keV emission in the LB and found a 2 σ upper limit of 270 counts s^{-1} sr^{-1} in the *ROSAT* $\frac{3}{4}$ keV band.[1] This band includes both the O VII triplet

and the O VIII Lyα line. They also fitted a "standard" 10^6 K CIE LB model assuming a path length of $\sim$65 pc and found a good match to the observed $\frac{1}{4}$ keV emission with an emission measure of 0.0024 cm^{-6} pc. This would generate only $\sim$47 counts s^{-1} sr^{-1} in the $\frac{3}{4}$ keV band, well within the 2 σ limit. For comparison, this model predicts 0.28 LU of O VII line emission, which is the dominant contribution to the $\frac{3}{4}$ keV band emission.

The *ROSAT* PSPC had insufficient spectral resolution to separate the O VII and O VIII emission lines from each other, the background continuum, and possible Fe L line emission. We therefore used the *Chandra* ACIS instrument to redo the SMV93 observations with higher spectral and spatial resolution. Our results were unfortunately affected by a large solar flare during part of the observation, the charge transfer inefficiency degradation experienced by the ACIS detectors early in the *Chandra* mission, and the somewhat higher than expected background. Despite these issues, we were able to clearly detect strong O VII and O VIII emission lines.

3. OBSERVATIONS AND DATA ANALYSIS

MBM 12 is a nearby high-latitude molecular cloud ($l, b = 159°.2, -34°$). The distance to MBM 12 is somewhat controversial. Hobbs et al. (1986) placed it at $\sim$65 pc based on absorption-line studies; this is revised to 60 ± 30 pc using the new *Hipparcos* distances for their stars. However, Luhman (2001), using infrared photometry and extinction techniques, found a substantially higher distance of 275 ± 65 pc. Andersson et al. (2002) found a similar distance (360 ± 30 pc) for most of the extincting material, but also found evidence for some material at $\sim$80 pc. As part of a much larger survey of Na I absorption toward nearby stars, Lallement et al. (2003) found foreground dense gas toward stars 90–150 pc distant in the direction of MBM 12. They also suggested that the distance discrepancy could be resolved if the molecular cloud MBM 12 is itself behind a nearby dense H I cloud. However, since we use it as an optically thick shadowing target, so long as MBM 12 is nearer than the nonlocal Galactic sources of $\frac{3}{4}$ keV band X-rays that contribute to the diffuse background, the precise distance is unimportant. Indeed, the greater distance is interesting because it would constrain possible sources of diffuse $\frac{3}{4}$ keV band X-rays.

Our *Chandra* observations of MBM 12 were separated into two nearly equal sections. The first observation (hereafter Obi0) was performed on 2000 July 9–10. This observation was cut short by a severe solar flare that led to an automatic shutdown. Preshutdown, the flare apparently also created a systematically higher background in the ACIS during the entire observation, which unfortunately meant the entire observation had to be excluded (see § 3.1). The second observation (hereafter Obi1), was performed on 2000 August 17 for $\sim$56 ks during a time of lower solar activity. The pointing direction for both observations was $02^h55^m50^s.2, 19°30'14''.0$ (see Fig. 1). The primary CCD, ACIS-S3, was placed on the peak of the 100 μm *IRAS* emission, which we assume corresponds to the densest part of the cloud.

MBM 12 is a relatively thin molecular cloud, and so we must consider whether it is optically thick to background X-rays even at the relatively soft energies of O VII ($\sim$0.57 keV) and O VIII (0.654 keV). Assuming solar abundances, the cross sections at these energies are 9.4×10^{-22} and 6.7×10^{-22} cm^{-2} per H atom, respectively (Balucinska-Church & McCammon 1992). Measuring the column density over the face of the entire cloud is difficult. Absorption-line measurements show the column density at one position; Luhman (2001) found that most stars in MBM 12 have $A_V < 2$, with background stars in the range $A_V = 3-8$. Converting this to an equivalent hydrogen column density via

---

[1] For consistency we present all surface brightnesses in units of steradians; note that 1 sr = 1.18×10^7 arcmin^2.
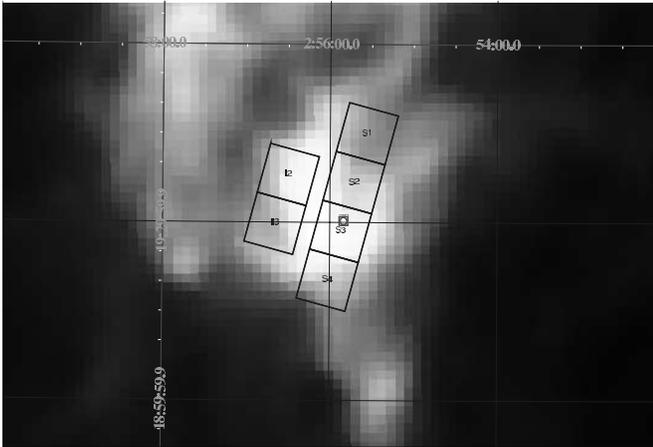
Fig. 1.—*IRAS* 100 μm image of MBM 12, with the *Chandra* observation coordinates overlaid. [*See the electronic edition of the Journal for a color version of this figure.*]

$N_H/A_V = 1.9 \times 10^{21}$ cm^{-2} mag^{-1} (Seward 2000) gives $N_H < 3.8 \times 10^{21}$ cm^{-2} for much of the cloud, with a maximum value in the range $N_H = (6–15) \times 10^{21}$ cm^{-2}. SMV93 also measured the column density by cross-correlating the *ROSAT* $\frac{3}{4}$ keV and *IRAS* 100 μm flux, and derived a value of $N_H/F(100~\mu\text{m}) = 1.3^{+1.1}_{-0.1} \times 10^{20}$ cm^{-2} (MJy sr^{-1})$^{-1}$. For these observations, the central ACIS-S3 detector was positioned on the brightest infrared position of MBM 12, where $F(100~\mu\text{m}) = 30–35$ MJy sr^{-1}, so using the SMV93 ratio, $N_H = (3.6–8.4) \times 10^{21}$ cm^{-2}. Since we are observing in the direction of the densest part of MBM 12, we believe that $N_H = 4 \times 10^{21}$ cm^{-2} is a conservative value. The opacity of MBM 12 to background line emission is then $\tau(\text{O VII}) = 3.76$ and $\tau(\text{O VIII}) = 2.68$, and any distant emission will be reduced by 98% at O VII and 93% at O VIII. Only an extremely bright background source could affect our results, and this is unlikely. The *ROSAT* PSPC had a large 2° field of view, and although SMV93 found some $\frac{3}{4}$ keV emission off-cloud, it was only ~3.3 times brighter than their 2 σ upper limit for the $\frac{3}{4}$ keV toward the cloud.

3.1. *Data Processing*

The data reduction process was somewhat unusual, since emission from the LB completely fills the field of view, and the features of interest are extremely weak. Our original plan was to use the front-illuminated (FI) CCDs to measure the individual lines, and the back-illuminated (BI) CCDs (which have more effective area but lower resolution and higher background) to

confirm the result. Based on the Gendreau et al. (1995) measurement of the soft X-ray background, we expected prelaunch to obtain at most ~0.004 counts s^{-1} from O VII and ~0.001 counts s^{-1} from O VIII lines from both the four (FI) ACIS-I CCDs and the (BI) ACIS S3 CCD. However, after the proton damage to the FI CCDs early in the mission, the highly row dependent response of the FI CCDs means that these lines would be very difficult to extract robustly. Therefore, we focused on data from the BI CCD ACIS-S3.

We used CIAO, version 3.1, tools to process the observations, along with CALDB, version 2.27. Our result depends crucially on the background measurement, which must be done indirectly since the source fills the field of view. The two most important steps are removing flares and point sources. We followed a procedure similar to that described in Markevitch et al. (2003), although as the data were taken in FAINT mode, VFAINT filtering was not possible. For the purposes of source-finding only, we merged the two observations using the *align_evt* routine.[2] We then ran *celldetect*, requiring a signal-to-noise ratio (S/N) > 3, which found 16 sources (including the well-known source XY Ari). We excluded all these sources, using circles of 15″ radius (except XY Ari, where we used a 30″ radius circle). This procedure eliminated 15% of all events, with XY Ari alone accounting for 11%, and removed 5.0% of the area, leaving a total field of view of 67 arcmin^2. We then made a light curve of the ACIS-S3 events between 2.5 and 7 keV for each observation, as shown in Figure 2. We constructed a histogram of the observed rates and fitted it with a Gaussian, representing the quiescent rate, plus a constant to roughly model the flares. We obtained good fits in both cases, which showed that the quiescent level in the first observation was 0.22 counts s^{-1}, while in the second it was 0.16 counts s^{-1}. The quiescent rate in the first observation is significantly above those shown in Markevitch et al. (2003), which ranged from 0.1 to 0.16 counts s^{-1}. These fluctuations in the background counting rate are likely due to protons that are trapped in the Earth's radiation belts or directly from solar flares.

Following Markevitch et al. (2003), we removed all times when the count rate was not within 20% of the average rate for the second observation. The maximum allowed rate is therefore 0.192 counts s^{-1}, which limits the first observation to 2.2 ks of "good time," too little data to be useful. This exclusion was not capricious. Although the first MBM 12 observation was ~40% brighter than the average background rate for ACIS-S3, we expended substantial effort attempting to model it. All our attempts required adding what amounted to arbitrary terms at the same

---

[2] See http://asc.harvard.edu/cont-soft/software/align_evt.1.6.html.
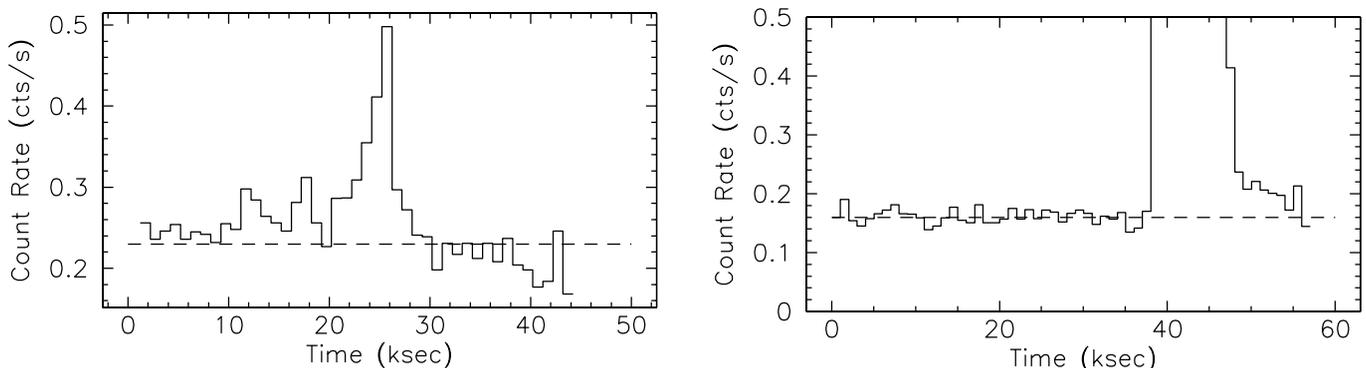
Fig. 2.—*Left*: Light curve from the first MBM 12 observation between 2.5 and 7 keV, with a dashed line showing our best-fit quiescent rate of 0.22 counts s^{-1}. *Right*: Same, from the second observation, with a quiescent rate of 0.16 counts s^{-1}.

TABLE 1
TOTAL COUNTS AND RATIOS IN SELECTED BANDS

	ObsID 62850		MBM 12 Obi1		"Good" Obi0		"All" Obi0	
BAND	Counts	Ratio	Counts	Ratio	Counts	Ratio	Counts	Ratio
PHA (2500–3000)	36,197	1.000	21,735	1.000	1407	1.000	75,925	1.000
0.5–2.0[a]........................	4762	0.132	4015	0.185	314	0.223	46,387	0.611
2.0–7.0[a]........................	8545	0.236	7492	0.344	513	0.365	63,693	0.839
5.0–10.0[a]......................	22,742	0.628	14,877	0.684	978	0.695	96,311	1.269

[a] In units of keV.

energies as our emission lines, so no conclusive results were possible. Therefore, we reluctantly excluded it from the remaining analysis. After filtering the second observation, we were left with 38.2 ks of usable data.

To cross-check these results, we followed Markevitch et al. (2003) and compared the total counts in selected energy bands to the total counts seen with pulse-height amplitude (PHA) values between 2500 and 3000. PHA values in this range correspond to energies above 10 keV, which are outside *Chandra*'s range and thus effectively measure the "particle background" rate. Table 1 shows the results for our MBM 12 observations and one of our background data sets, ObsID 62850 (see § 3.2). In Table 1 we show the results from the filtered Obi1 data as well as the 2.2 ks of "good" data from Obi0 and values from all of Obi0. Ratios of the number of events in these bands to the number of events with PHA values between 2500 and 3000 are given as well. The unfiltered Obi0 data show very high ratios, suggesting contamination from some source besides the normal particle background. Conversely, the Obi1 observations of MBM 12 show slightly higher ratios compared to the ObsID 62850 ratios, consistent with a weak source such as the diffuse X-ray background. The ratios seen for ObsID 62850 are similar to the average values observed by Markevitch et al. (2003) for the EHM observations.

3.2. *Background*

Since the LB fills the field of view in all normal *Chandra* observations, determining the true background is nontrivial. There are three types of *Chandra* observations that contain only instrumental or near-Earth background: the Dark Moon observation described in Markevitch et al. (2003), the event histogram mode (EHM) data taken by ACIS during HRC-I observations and also described in Markevitch et al. (2003), and the "stowed ACIS" observations first described in Wargelin et al. (2004). These latter observations (to date, ObsID 4286, 62846, 62848, and 62850) were done with ACIS clocking the CCDs in "timed exposure" mode and reporting event data in the VFAINT telemetry format, and with ACIS in a stowed position at which ACIS receives negligible flux from the telescope and the onboard calibration source. We used data from ObsIDs 62848, 62848, and 62850 as our background data sets. Together these data sets represent 144 ks of observations, although they were treated independently in our fits. ObsID 4286 is less than 10 ks and was not used. Between our observations and the last of these observations (in 2003 December) there was little change in the overall background rate.[3]

We fitted the MBM 12 data from Obi1 simultaneously with stowed ACIS data using both a foreground and background model and Sherpa's CSTAT statistic. The fits were restricted to the range 0.4–6 keV, since above 6 keV the background appears to rise because of the near-constant cosmic-ray background combined with the falling mirror response, while below 0.4 keV the background rises and falls in a highly variable fashion. Our foreground model consisted of two unabsorbed delta functions for the O VII and O VIII lines, plus an absorbed power law and thermal component to represent the cosmic X-ray background and the distant hot Galactic component. We did not include a thermal component with $T \sim 10^6$ K to represent the LB emission, as nearly all of that emission would be below 0.4 keV, except for the oxygen lines. The absorption was allowed to vary between $N_H = 3.6$ and 8.4×10^{21} cm^2 for both components; the best-fit value was 6×10^{21} cm^2, although our results were not particularly sensitive to this value. We used the values from Lumb et al. (2002) for the power-law component ($\Gamma = 1.42 \pm 0.03$, normalized to $8.44^{+2.55}_{-0.23}$ photons cm^{-2} s^{-1} keV^{-1} at 1 keV), as well as for the temperature of the thermal component (0.2 ± 0.01 keV). The normalization on the thermal component was allowed to vary, since significant variation has been seen for this absorbed hot gas (Kuntz & Snowden 2000). The O VIII Lyα line position was set at 0.654 keV. However, since the O VII emission is from a triplet of lines whose dominant member is unknown, we allowed the centroid of the line complex to float within a range of O VII line positions between the forbidden line at 0.561 keV and the resonance line at 0.574 keV. We found that the sharp rise seen below 0.5 keV in both the source and background could be fitted using a low-energy Lorentzian, and we also included delta functions at 1.78 keV (Si-K) and 2.15 keV (Au-M) to fit the particle-induced fluorescence seen at these energies. Finally, the particle-induced continuum background was modeled as a line with slope and offset, which was not folded through the instrumental response.

4. RESULTS

Since we used the standard model of the diffuse X-ray background, we were not surprised to find a good fit to the data. The source model had only three significant parameters: the O VII and O VIII line fluxes, and the normalization on the absorbed Galactic thermal component. The total absorbed flux from this last component was only $F_X(0.4–6 \text{ keV}) = 0.066$ photons cm^{-2} s^{-1} sr^{-1}, significantly less flux than from either of the two oxygen lines. Our results for the line emission are shown in Figure 3 and Table 2. Table 2 also lists O VII and O VIII fluxes measured at high Galactic latitude with *ASCA* (Gendreau et al. 1995) and XQC (McCammon et al. 2002). In addition, line fluxes due to heliospheric charge exchange (Snowden et al. 2004, hereafter SCK04) and geocoronal charge exchange (Wargelin et al. 2004, labeled "Dark Moon"; see § 5.1) are listed, along with the 2 σ upper limits from the *ROSAT* observations of MBM 12 (SMV93). The listed errors are 1 σ, except for the Wargelin et al. (2004) data, where the 90% likelihood range is shown. The SMV93 limits
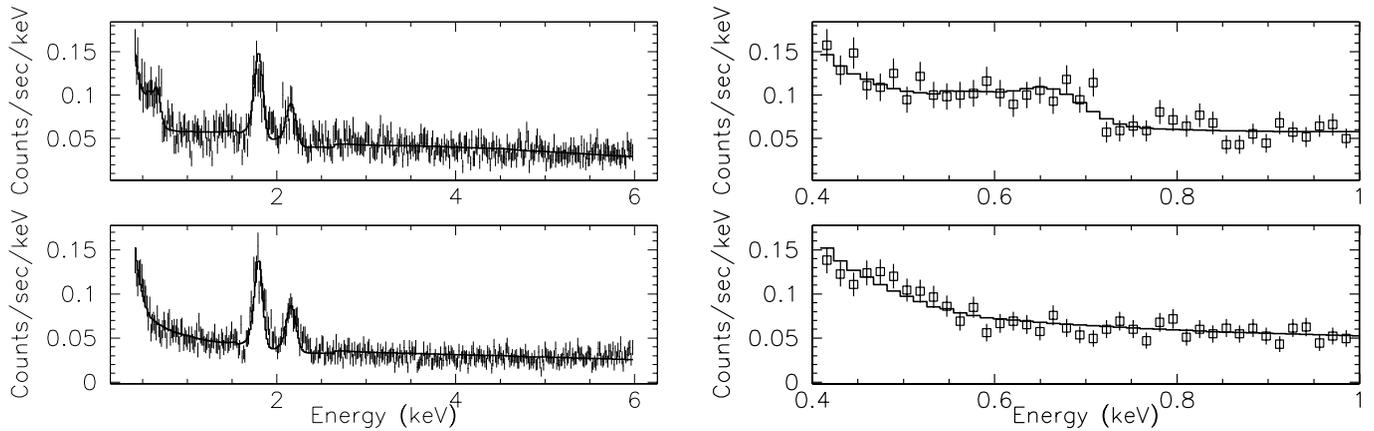
Fig. 3.—*Top left*: Best-fit spectrum for MBM 12 observation. *Bottom left*: Best-fit background spectrum from ObsID 62850; note the fluorescence lines at 1.78 and 2.15 keV. *Top right*: Best-fit spectrum from MBM 12 between 0.4 and 1 keV, showing the strength of the oxygen lines. *Bottom right*: Same, showing the background fit.

assume all the emission is from that one line, since *ROSAT* could not resolve O VII from O VIII. When we allowed the O VII line to float between the forbidden and resonance line energies, we found that any value would lead to acceptable fits. The statistics and CCD resolution could not distinguish between either the low- or high-energy end, so our results are shown for an assumed "average" line position of 0.57 keV. Our best-fit O VII flux is consistent with the high-latitude Gendreau et al. (1995) results. However, the O VIII emission is significantly larger than the results of Gendreau et al. (1995) or McCammon et al. (2002). The strength of the O VIII is not strongly dependent on the details of background subtraction, since it is far from the rapidly rising background found at low energies on ACIS-S3. We conclude that this measurement is correct, but contaminated with solar system emission from charge exchange. Other measurements in Table 2 show that charge exchange can easily swamp any LB emission. For example, the Wargelin et al. (2004) "bright" results from the dark Moon (from their Table 7) are significantly larger than either our results or those of Gendreau et al. (1995), and the same is true of the SCK04 results.

5. DISCUSSION

Our original goal was to determine the age of the LB by measuring the ratio of the O VII and O VIII emission lines. In equilibrium, the O VIII emission would be negligible. A number of nonequilibrium models, however, predict detectable O VIII. Smith & Cox (2001) considered a range of models involving a series of supernova explosions. If the LB is still evolving 3–7 Myr after the last explosion, then their Figure 13*b* suggests that the O VIII would still be detectable relative to the O VII emission.[4] Alternatively, Breitschwerdt & Schmutzler (1994) and Breitschwerdt (2001) would also imply a detectable amount of O VIII emission

---

[4] Note that in Smith & Cox (2001) Figs. 11, 12, 19, and 20 are incorrect; they should be reduced by a factor of 4π because of an error by the author.

(see § 5.3). Solar flares, the variable response of the ACIS-I, and complicated background of the ACIS-S3 CCD have proved significant but not insurmountable obstacles. However, the strong O VIII line is a much larger problem, since it is significantly larger than has been measured at high latitudes that include both the LB and Galactic halo emission. As stated above, it seems likely that our results have been contaminated by charge exchange with the solar wind.

5.1. *Charge Exchange*

Charge exchange, as first noted by Cox (1998), is a serious complication for diffuse soft X-ray background studies. Charge exchange creates X-rays when electrons jump from neutral material (usually hydrogen or helium atoms) to excited levels of highly ionized atoms. Charge exchange between neutral H and O^{+7}, for example, can create O VII emission. The highly charged ions come from the solar wind and coronal mass ejections (CMEs). The neutral material can come from either the geocorona or the interstellar medium as it flows into the heliosphere; see Cravens (2000) for an overview of this mechanism. Cravens et al. (2001) show that the so-called long-term enhancements (LTEs) observed during the *ROSAT* sky survey, which were apparent brightenings of the diffuse X-ray sky lasting days to weeks, can be explained by X-ray emission from charge exchange between the solar wind and either the geocorona or the interstellar medium, or both.

Wargelin et al. (2004) detected a strongly time-dependent O VII line along with weaker O VIII emission from *Chandra* observations of the dark Moon. The source of these X-rays is almost certainly charge exchange between solar wind ions and the geocorona. The time variability of the solar wind makes the time dependence of the X-ray emission understandable. Detailed spectral models of charge exchange emission have been developed (e.g., Kharchenko & Dalgarno 2001). Wargelin et al. (2004) used these calculations to model the O VII and O VIII geocoronal emission as a function of the solar wind oxygen ion flux (which can be

TABLE 2
OXYGEN LINE EMISSION

Ion	This Work (LU)	*ASCA* (LU)	XQC (LU)	SCK04 (LU)	Dark Moon (LU)	SMV93 (LU)
O VII	1.79 ± 0.55	2.3 ± 0.3	4.8 ± 0.8	7.39 ± 0.79	6.5–13.6	<7.1
O VIII..................	2.34 ± 0.36	0.6 ± 0.15	1.6 ± 0.4	6.54 ± 0.34	2.7–6.1	<3.6

estimated from *ACE* measurements). Their model estimates the surface brightness in each line as

$$L_S = \frac{v_c n_p f_O y_{il} \sigma_i n_{n0}}{4\pi} \, 5R_{\rm E} \left(\frac{10R_{\rm E}}{r_{\rm min}}\right)^2, \quad (1)$$

where v_c is the solar wind velocity, n_p is the proton density, f_O is the relative abundance of oxygen, y_{il} is the line yield per charge exchange, σ_i is the charge exchange cross section, and n_{n0} is the neutral particle density at 10 Earth radii ($R_{\rm E}$); $r_{\rm min}$ is the geocentric distance to the edge of the magnetosphere or the spacecraft position, whichever is farther. Some of these parameters are measured by *ACE*.[5] This model predicts that the O VIII/O VII ratio due solely to charge exchange is $1.36(n_{\rm O^{+8}}/n_{\rm O^{+7}}) + 0.14$, where n_I is the density of ion I. This result uses values from Tables 5 and 6 of Wargelin et al. (2004) and including the O VII Kβ line in the O VIII emissivity, since they would be blended. In a typical slow solar wind, $n_{\rm O^{+8}}/n_{\rm O^{+7}} \approx 0.35$, implying a ratio of 0.616 (SCK04). Unfortunately, *ACE* does not yet routinely provide measurements of $n_{\rm O^{+8}}/n_{\rm O^{+7}}$, as it does with $n_{\rm O^{+7}}/n_{\rm O^{+6}}$. During Obi1, $n_{\rm O^{+7}}/n_{\rm O^{+6}}$ was $\sim$0.7, approximately midway between the average value for the slow solar wind ($\sim$0.3) and the value of $\sim$1.4 measured during the brightest dark Moon observations.

Going beyond the Earth-Moon system, the time-variable effects of charge exchange in the broader heliosphere were measured by SCK04. They used a series of four *XMM-Newton* observations of the Hubble Deep Field–North (a high-latitude patch of sky devoid of bright X-ray sources) to measure O VII and O VIII emission and correlated their results with solar wind observations from *ACE*. They found that three out of four observations (as well as part of the fourth) agreed with the standard diffuse X-ray background model, and that during these times the proton flux and $n_{\rm O^{+7}}/n_{\rm O^{+6}}$ ratios in the solar wind were $(1.5\text{–}3.2) \times 10^8$ cm^{-2} s^{-1} and 0.15–0.46, respectively. However, part of the fourth observation showed substantially brighter O VII and O VIII, as well as sharp increases in both the proton flux (to 8.0×10^8 cm^{-2} s^{-1}) and the $n_{\rm O^{+7}}/n_{\rm O^{+6}}$ ratio (to 0.99). Their measured heliospheric surface brightnesses are given in Table 2.

Our viewing geometry for MBM 12 during Obi1 is such that we would expect an effect due to charge exchange, especially for O VII. The heliospheric "downstream" direction, with respect to the Sun's motion through the Local Cloud is centered around ecliptic coordinates $74°.5, -6°$ (Lallement & Bertin 1992), which corresponds to December 5 for the Earth's orbital position. MBM 12 ($47°.6, +3°$ in ecliptic coordinates) is not far from this direction, so when Obi1 was done on August 17 it should have been viewing a sparse column of neutral heliospheric gas— mostly He, since the H would be largely ionized as it flowed by the Sun. From Table 9 of Wargelin et al. (2004), we therefore expect, for a typical slow solar wind, a total *ROSAT* surface brightness of $\sim$470 counts s^{-1} sr^{-1}. The geocoronal component should be roughly one-fourth of this, as the viewing direction is (roughly) through the flank of the magnetopause, again from Table 9 of and Figure 7 of Wargelin et al. (2004). We therefore expect that the total surface brightnesses will be $\sim$5 times the geocoronal model values in Table 8 of Wargelin et al. (2004), or 1.4 and 0.56 photons cm^{-2} s^{-1} sr^{-1} for O VII and O VIII, respectively. Given the uncertainties, and the expectation that charge exchange emission does not account for the entire soft X-ray background observed by *ROSAT* (but see Lallement 2004), the O VII prediction matches our result well, but the O VIII is still anomalously high for a typical slow solar wind alone.

However, in addition to the solar wind, it should be noted that there were a number of halo CME events during 2000 July.[6] These would have the effect of mixing into the Earth's side of the interplanetary medium some CME plasma that may well have a substantially higher ionization state. These vary from event to event, and there are only a few events that are suitable for study both in the near-Sun environment with *SOHO* and in situ with a solar wind ion charge state spectrometer.

For example, one such event was observed in 2002 November and December (Poletto et al. 2004). The UVCS data measured remotely by *SOHO* at 1.7 $R_\odot$ above the solar limb show lines of Fe XVIII, and the SWICS data measured in situ by *Ulysses* also show high ions of iron (Fe^{+16} being prominent). This leads these authors to conclude that, for this CME event, the ionization state is characteristic of a "freezing in" temperature in excess of 6 MK. At such temperatures, oxygen is fully ionized.

Cravens (2000) argues that solar wind charge exchange with the neutral interstellar medium (ISM) mostly occurs at distances of a few AU from the Sun because of the depletion of neutral gas near the Sun. Since 100 km s^{-1} translates to about 1.7 AU per month, and CME fronts range from about 20 to over 2000 km s^{-1} (Webb 2002), we are not concerned with a single event but an average over the week or two prior to the observation.

We therefore conclude that the large O VIII/O VII ratio we observe could be expected from the charge exchange of CME plasma with the neutral ISM, but that the details are sufficiently complex (and the data sufficiently sparse) that prediction of this ratio is difficult to impossible. We can say, however, that the observed O VII and O VIII provides a (weak) upper limit to the emission from the LB.

5.2. *Collisional Models*

What do these observations imply if the observed line emission is due to electron/ion interactions rather than charge exchange? In this case it is relatively easy to calculate the expected contribution from each atomic process. O VII emission from any of the triplet of lines is created by direct excitation (where we include cascades from excitation to higher levels), electron recombination onto O^{+7}, or inner-shell ionization of O^{+5}. O VIII lines come from direct excitation or recombination from bare oxygen ions; K-shell ionization of O^{+6} does not have a large cross section for emitting O VIII. If the plasma is at or near ionization equilibrium, then we can ignore blending from satellite lines or other emission lines in the region of interest, as they should contribute only a small fraction of the total emission; we consider the far from equilibrium case in § 5.3. For example, at CCD resolution the O VII $1s3l \rightarrow 1s^2$ line will blend with the O VIII Lyα line. However, it contributes at most 6% of the flux of the O VIII Lyα line and so can be ignored to a first approximation.

With these assumptions, the observed line surface brightness (in LU) along a particular line of sight can be written as

$$L_S(\text{O VII}) = \frac{1}{4\pi} \int dR \, \frac{n_e^2(r)}{1.2} \left[n_{+5}(r)\Lambda_{\rm O\,VII}^{\rm IS}(T) \right.$$
$$\left. + n_{+6}(r)\Lambda_{\rm O\,VII}^{\rm DE}(T) + n_{+7}(r)\Lambda_{\rm O\,VII}^{\rm RC}(T) \right], \quad (2)$$

$$L_S(\text{O VIII}) = \frac{1}{4\pi} \int dR \, \frac{n_e^2(r)}{1.2} \left[n_{+7}(r)\Lambda_{\rm O\,VIII}^{\rm DE}(T) \right.$$
$$\left. + n_{+8}(r)\Lambda_{\rm O\,VIII}^{\rm RC}(T) \right], \quad (3)$$

---

[5] Data available at http://www.srl.caltech.edu/ACE.

[6] See catalog at ftp://lasco6.nascom.nasa.gov/pub/lasco/status/LASCO_CME_List_2000.
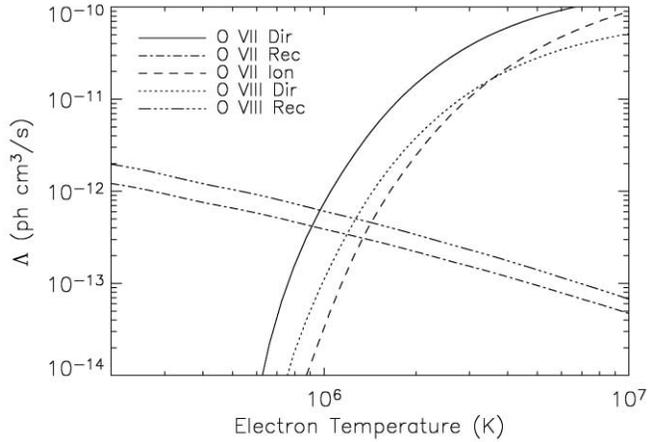
Fig. 4.—Shows Λ curves as a function of electron temperature, using APEC and data from ATOMDB, ver. 1.3.1. The total emission from each process is $n_e n_I \Lambda$.

where L_S is in LU, $n_e(r)$ is the electron density at distance r, and $n_{+n}(r)$ is the ion density of O^{+n} at r. We also assume that the hydrogen and helium are fully ionized, so $n_e \approx 1.2 n_H$; $\Lambda_I^{IS}(T)$, $\Lambda_I^{DE}(T)$, $\Lambda_I^{RC}(T)$ are the rate coefficients (in $cm^3\ s^{-1}$) for creating an emission line via inner shell, direct excitation, or recombination for ion I, and are plotted in Figure 4.

Since four different ions may be involved in creating O VII and O VIII emission lines, we cannot uniquely solve for the density, temperature, and ionization state of the system. However, we can easily show that these line fluxes are not commensurate with an equilibrium plasma. The O VIII flux provides the strongest limit, as this line is not expected in an equilibrium model for the LB. Figure 4 shows that the direct excitation rate for this line rises rapidly with temperature, so a higher temperature will produce more O VIII. Based on the Kuntz & Snowden (2000) survey of LB results (see their Table 1), we assume that the allowed electron temperature in the LB is $< 2 \times 10^6$ K; in equilibrium at this temperature, $n_{O^{+6}}/n_{O^{+7}} > 1$. Figure 4 clearly shows that the direct excitation rate for O VII is more than triple the rate for O VIII excitation, which would predict O VII/O VIII > 3, in strong contrast to our result. Therefore, either the O VIII line emission is not coming from the LB, or the plasma is recombining, with significantly more O^{+7} or O^{+8} ions than O^{+6} ions. We consider some aspects of this possibility below.

5.3. Recombining Plasma Models

Breitschwerdt & Schmutzler (1994) proposed a radical new model for the LB suggesting that it was not in fact "hot," but rather the X-ray emission was created by recombination of highly ionized atoms with cool (10^4 to 3×10^5 K) electrons. Their model assumes that the LB was a preexisting cavity, probably formed by earlier supernova explosions and possibly associated with the Sco-Cen superbubble. Then, inside this cavity a few million years ago, a massive star inside a dense cloud exploded. After the supernova shock-heated and ionized the entire cloud, the resulting hot ions expanded into the low-density cavity and cooled adiabatically. This model was partially inspired by the relatively high average density of 0.024 cm^{-3} measured from a nearby (130 pc distant) pulsar's dispersion measure (Reynolds 1990). If this density is representative of the LB as a whole, then an $\sim 10^6$ K plasma would create far more soft X-rays than are observed. Breitschwerdt & Schmutzler (1994) showed that a low-temperature, high-ionization state plasma with this den-

sity could generate the observed $\frac{1}{4}$ keV X-ray emission. Later papers (Breitschwerdt et al. 1996; Breitschwerdt 2001) have described the model in more detail and made predictions of the flux in various bandpasses. This model also naturally explained the existence of the "Local Fluff," neutral H I clouds (e.g., Bochkarev 1987; Frisch 1995), which are hard to understand in the context of hot bubble models.

Although more complicated than the equilibrium isothermal LB model, a strength of this model is that it does not require a particular fine-tuning or a complicated mix of hydrodynamic and plasma models. As noted by Breitschwerdt (2001), only some basic input parameters—cavity radius R, electron density n_e, electron temperature T_e, and evolution time t—are needed, and a fairly wide range of these values matched the available data at the time.

However, FUSE observations (Shelton 2003) put a surprisingly low 2 σ upper limit on the O VI $\lambda\lambda 1032$, 1038 emission from the LB of 500 and 530 LU, respectively, and 800 LU for both lines combined. Shelton (2003) noted that this result alone strongly constrains any recombining plasma model and, when combined with other discrepancies in the C III emission and the N(O VI) column density, "practically eliminate[s] this class of models." However, this argument rests on discrepancies in two unrelated ions, O VI and C III, leaving open the possibility that these issues could be finessed with the correctly tuned input parameters. Recombining plasma models are still being invoked in recent papers (e.g., Freyberg et al. 2004; Hurwitz et al. 2005). The O VI upper limits are quite stringent, however, and combining them with our measurements allows a rigorous test of the model using all relevant oxygen ions as they recombine from fully stripped O^{+8} to O^{+5} and beyond. Any acceptable recombining plasma model would have to match the upper limits found for each ion's emission lines, while also emitting at least some of the observed $\frac{1}{4}$ keV band X-rays.

Interestingly, in the case of a purely recombining plasma, the ionization state of the plasma at any point in its evolution can be calculated analytically. If ionization can be ignored, then the population of any ion state can be written as

$$\frac{dp^i}{dt} = -R_i n_e p^i + R_{i+1} n_e p^{i+1}, \quad (4)$$

where p^i is the population of the ion with i electrons and R_i is the recombination rate (in $cm^3\ s^{-1}$) from the ith ion state to the $i + 1$ state. In the case of the fully stripped ion (p^0), the second term in equation (4) is zero, as there is no higher ion. Equation (4) then leads to a linked series of first-order differential equations that can be easily solved. Assuming that initially the population is fully stripped [$p^0(0) \equiv 1$], the population of any ion can be written as

$$p^i = \sum_{j=0}^{i-1} \left\{ \frac{R_{i-1} f_j^{i-1}}{R_i - R_j} \left[\exp\left(-R_j n_e t\right) - \exp\left(-R_i n_e t\right) \right] \right\}, \quad (5)$$

where f_j^i equals 1 when $i = j = 0$ and is otherwise defined by the recursion relation:

$$f_j^i = \begin{cases} \dfrac{R_{i-1} f_j^{i-1}}{R_i - R_j} & \text{if } j < i, \\[3ex] -\displaystyle\sum_{j=0}^{i-1} \dfrac{R_{i-1} f_j^{i-1}}{R_i - R_j} & \text{if } j = i. \end{cases} \quad (6)$$
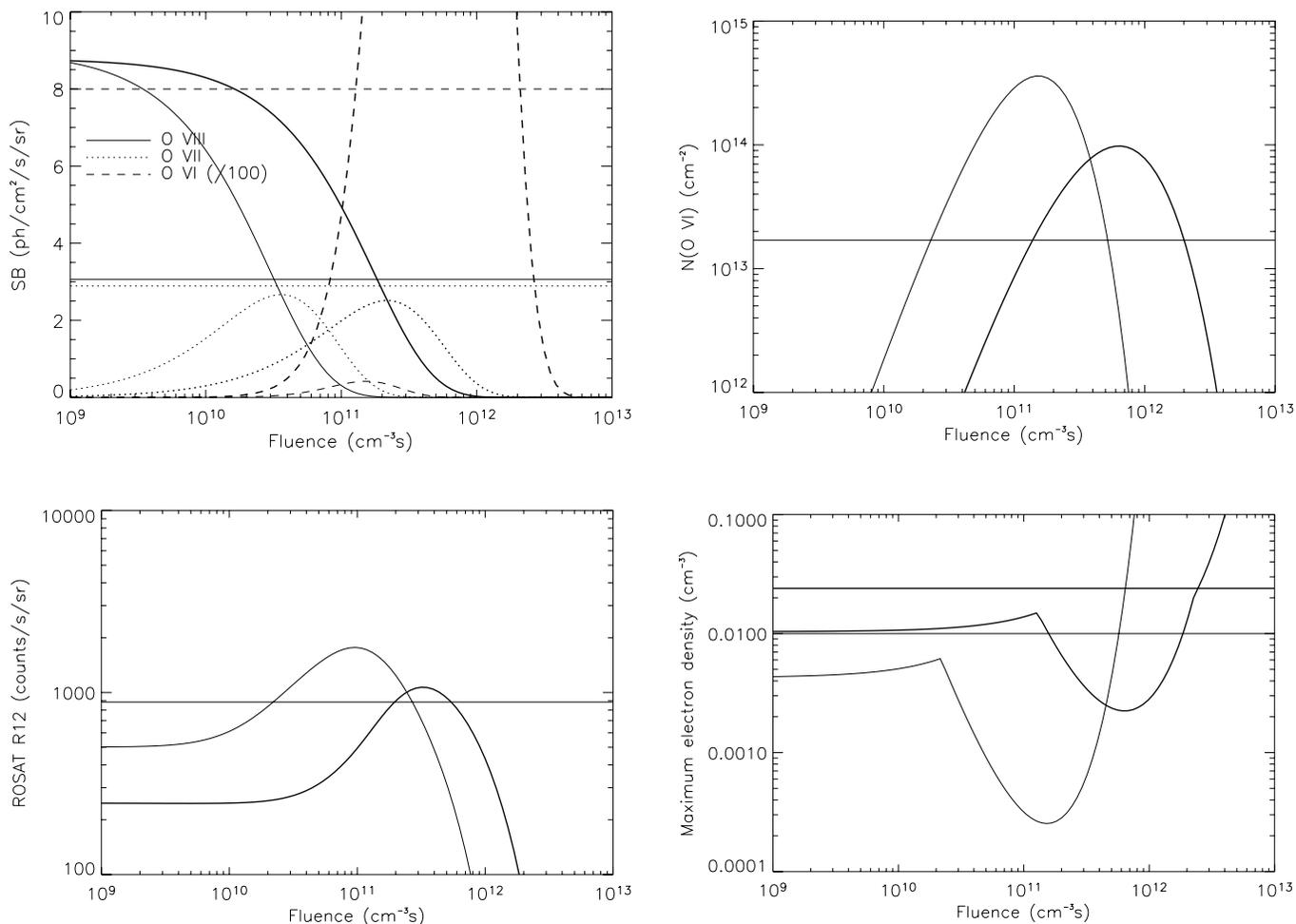
Fig. 5.—*Top left*: O VIII Lyα, O VII triplet, and O VI doublet emission and observed upper limits for two different models as a function of fluence. Thick curves show a model with $R = 114$ pc, $n_e = 0.024$ cm^{-3}, and $T_e = 3 \times 10^5$ K; thin lines are for a model with $R = 114$ pc, $n_e = 0.01$ cm^{-3}, and $T_e = 2 \times 10^4$ K. *Top right*: O VI column density in the LB for the same models, along with the observed upper limit from the LB. *Bottom left*: *ROSAT* R12 emission from both models, with a line showing our estimated lower limit. *Bottom right*: Maximum allowed electron density for a 114 pc bubble in either model, based only on the O VIII, O VII, and O VI limits. The effects of each oxygen ion's limit are visible. Except at large fluences (when the R12 emission is negligible), the maximum allowed density is less than the assumed model density, showing why these models are excluded.

To calculate R_i we used radiative recombination rates from Verner & Ferland (1996) and dielectronic rates from Romanik (1988, 1996). Combining this with Figure 4 we can calculate the predicted O VIII Lyα and O VII triplet flux due to recombination for any temperature and density. We calculated the O VI flux from electron collisions (recombination from O^{+6} was negligible) using the collision strengths from Griffin et al. (2000).

However, the upper limits on the O VIII, O VII, and O VI emission and the N(O VI) column density were not sufficient, as a sufficiently low density would always be allowed (see Fig. 5, *bottom right*). The recombining ion model, however, was initially developed with a relatively high density in mind and tested against the observed $\frac{1}{4}$ keV band emission. We have developed an approximate but robust model of the X-ray spectrum from a recombining plasma to compare to the *ROSAT* R12-band emission. This model considered only emission from dielectronic and radiative recombination, omitting direct excitation. In a plasma with low electron temperature, the radiative recombination continuum appears as a nearly linelike (width $\sim kT$) feature at the binding energy of the recombined level. We therefore assumed that each radiative recombination led to a photon at the binding energy of the ion; this ignores cascades, which would modify somewhat the exact distribution of the photons but is reasonably accurate for our purposes. The dielectronic satellite lines were

calculated using data from Romanik (1988, 1996). We then folded the resulting spectrum between 50 and 1000 eV through the *ROSAT* R12-band response to calculate the expected emission in this band.

For the O VII and O VIII limits we used the 2 σ upper limits from the MBM 12 observation, despite our strong suspicion (based on the *ACE* data and the odd ratio of the two lines) that these are already contaminated by charge exchange. In addition, in the case of O VIII our 2 σ upper limit is larger than the value observed by XQC (McCammon et al. 2002) over a 1 sr field of view, which necessarily includes both LB and more distant emission. Therefore, we feel that this is a very conservative upper limit to the local contribution from O VII and O VIII.

Defining an "upper limit" to the column density of O VI in the LB is difficult, and so we attempted to determine a reasonable value by indirect methods. Shelton & Cox (1994) found through a statistical analysis that the most likely value for N(O VI) in the LB was 1.6×10^{13} cm^{-2}. The *Copernicus* data this was based on (Jenkins 1978) also shows that no O or B star within 250 pc has a column density greater than this value. In addition, *FUSE* results toward 25 nearby white dwarfs (Oegerle et al. 2005) show at most 1.7×10^{13} cm^{-2}, with an average value of $\sim 7 \times 10^{12}$ cm^{-2}. We therefore chose N(O VI) $< 1.7 \times 10^{13}$ cm^{-2} as our upper limit to the column density of O VI through the LB.

We wanted to choose a very conservative value for the minimum R12-band emission from the LB required by the model. Breitschwerdt & Schmutzler (1994) assumed that some of the observed soft X-ray emission came from distant superbubbles, since *ROSAT* had recently seen clouds in absorption. Nonetheless, they also required some local emission, although the required amount was somewhat uncertain. Since then, Kuntz et al. (1997) studied the foreground X-ray emission by analyzing the shadows seen by *ROSAT* toward nearby molecular clouds. They measured the foreground R12 emission seen toward nine clouds, finding a range of 3790–6190 counts s^{-1} sr^{-1}. This was followed by the exhaustive study of X-ray shadows by Snowden et al. (2000), who examined 378 clouds seen with *ROSAT*. Their results showed substantial variation from position to position, with a mean and standard deviation of 5810 ± 1960 counts s^{-1} sr^{-1}. Based on these results, we decided to require at least 910 counts s^{-1} sr^{-1} in the R12 band, far below the value found by Kuntz et al. (1997) and $2.5\,\sigma$ below the Snowden et al. (2000) mean value.

In Figure 5 we show the predicted O VIII, O VII, and O VI emission, the O VI column density, the R12 emission for two recombining plasma models, and the maximum allowed electron density based solely on the oxygen ion upper limits for both models. The oxygen, neon, and argon abundances were taken from Asplund et al. (2004), with all other abundances taken from Anders & Grevesse (1989). The plots are shown as functions of the fluence ($\equiv n_e t$), a convenient variable as all the rates are proportional to the electron density. The thick curves show the results for the model described in Breitschwerdt (2001), with a cavity radius of 114 pc, an electron density of 0.024 cm^{-3}, and an electron temperature of 3×10^5 K. Note how the R12 emission matches the observations over a wide range of fluences, suggesting that our $\frac{1}{4}$ keV emission model agrees with that used in Breitschwerdt (2001). Whenever the R12 emission reaches and exceeds the lower limit in this model, however, the O VI emission exceeds its upper limit. The thin curves show a second model, with the same radius, an electron density of 0.01 cm^{-3}, and an electron temperature of 2×10^4 K. In this case there is a small region with fluence $\sim 10^{10}$ cm^{-3} s, where the R12 and O VI emission pass their lower and upper limits, respectively. However, in this range the predicted O VII and O VIII substantially exceed the upper limits toward MBM 12. At later fluences the predicted O VII and O VIII emission drops, but the N(O VI) column density exceeds the observed value. In sum, there is no point that simultaneously meets all the upper and lower limits.

The R12 emission calculation is necessary, since it provides the only lower limit, but it is also quite complex to calculate, and it is useful to consider what can be derived purely from the simpler oxygen ions. Figure 5 (*bottom right*) plots the limit on the electron density available purely from the oxygen emission and absorption upper limits. For example, the O VIII emission is given by

$$\text{O VIII} = n_e n_{+8} \frac{R}{4\pi} \Lambda^{\text{RC}}_{\text{O VIII}}(T), \qquad (7)$$

which can easily be converted into an upper limit on the electron density, since the remaining terms are determined by re-

combining ion model. As can be seen in the model, the limits from the oxygen ions alone require the electron density to be below the assumed density until very late times or fluences.

We have examined a wide range of input parameters for the recombining plasma model. We considered electron densities up to 0.03 cm^{-3}, electron temperatures in the range 10^4 to 5×10^5 K, and all cavity radii between 30 and 300 pc, and followed each set of values for 10^7 yr, the maximum plausible lifetime of the LB. Although the results vary substantially with the input parameters, as shown in Figure 5, none of our input parameters lead to predicted values that can simultaneously match these observational limits. In essence, the R12 lower limit requires a minimum density of highly ionized ions, while the tight observational limits on O VI, O VII, and O VIII simultaneously limit the density of these ions. We can with confidence dispose of at least the static recombining plasma model.

6. CONCLUSIONS

We have observed the nearby molecular cloud MBM 12 with *Chandra* and measured the foreground O VII and O VIII surface brightness toward the cloud, which should absorb any distant emission. Our observed values are higher than expected, and it appears likely, based on the *ACE* data, that charge exchange in the heliosphere or geocorona has contaminated our results. We measure a unexpectedly low ratio of O VII/O VIII = 0.76 ± 0.26, which is hard to understand in the context of other measurements or most LB models. In addition, circumstantial evidence also suggests that our results could be contaminated by charge exchange.

Despite this limitation, we are able to combine our upper limits with results from *FUSE* on O VI emission and absorption and the $\frac{1}{4}$ keV *ROSAT* R12 emission to reject the constant temperature recombining plasma model originally proposed by Breitschwerdt & Schmutzler (1994) over a wide range of input parameters. Since the sole moderate-resolution spectrum of the LB taken by DXS showed that the constant temperature equilibrium model could also be rejected (Sanders et al. 2001), this result implies that more complex models of the soft X-ray emission from the LB are required.

A number of more complex models have been proposed, however (e.g., Smith & Cox 2001; de Avillez & Breitschwerdt 2003), and selecting among the various possibilities will require high-resolution observations. If, for example, we could resolve the O VII triplet, then we would be able to determine whether the plasma is ionizing, recombining, or both in different regions. Although *Astro-E2* will have the necessary resolution, its effective area–solid angle product is only ~ 330 cm^2 arcmin^2, compared to $\sim 20{,}000$ cm^2 arcmin^2 for ACIS-S3. *Constellation-X*, however, will be a powerful instrument for understanding the recent history of our local environment.

REFERENCES

Acton, L. W., & Brown, W. A. 1978, ApJ, 225, 1065
Anders, E., & Grevesse, N. 1989, Geochim. Cosmochim. Acta, 53, 197
Andersson, B.-G., Idzi, R., Uomoto, A., Wannier, P. G., Chen, B., & Jorgensen, A. M. 2002, AJ, 124, 2164
Asplund, M., Grevesse, N., Sauval, A. J., Allende Prieto, C., & Kiselman, D. 2004, A&A, 417, 751

Balucinska-Church, M., & McCammon, D. 1992, ApJ, 400, 699
Bochkarev, N. G. 1987, Ap&SS, 138, 229
Bowyer, C. S., Field, G. B., & Mack, J. E. 1968, Nature, 217, 32
Breitschwerdt, D. 2001, Ap&SS, 276, 163
Breitschwerdt, D., Egger, R., Freyberg, M. J., Frisch, P. C., & Vallerga, J. V. 1996, Space Sci. Rev., 78, 183

Breitschwerdt, D., & Schmutzler, T. 1994, Nature, 371, 774

Bunner, A. N., Coleman, P. L., Kraushaar, W. L., McCammon, D., Palmieri, T. M., Shilepsky, A., & Ulmer, M. 1969, Nature, 223, 1222

Cox, D. P. 1998, in IAU Colloq. 166, The Local Bubble and Beyond, ed. D. Breitschwerdt, M. J. Freyberg, & J. Trümper (Berlin: Springer), 121

Cox, D. P., & Anderson, P. R. 1982, ApJ, 253, 268

Cravens, T. E. 2000, ApJ, 532, L153

Cravens, T. E., Robertson, I. P., & Snowden, S. L. 2001, J. Geophys. Res., 106, 24883

Davidsen, A., Henry, J. P., Middleditch, J., & Smith, H. E. 1972, ApJ, 177, L97

de Avillez, M. A., & Breitschwerdt, D. 2003, Rev. Mex. AA Ser. Conf., 15, 299

Edgar, R. J., & Cox, D. P. 1993, ApJ, 413, 190

Freyberg, M. J., Breitschwerdt, D., & Alves, J. 2004, Mem. Soc. Astron. Italiana, 75, 509

Frisch, P. C. 1995, Space Sci. Rev., 72, 499

Gabriel, A. H., Bely-Dubau, F., Faucher, P., & Acton, L. W. 1991, ApJ, 378, 438

Gendreau, K. C., et al. 1995, PASJ, 47, L5

Griffin, D. C., Badnell, N. R., & Pindzola, M. S. 2000, J. Phys. B, 33, 1013

Hobbs, L. M., Blitz, L., & Magnani, L. 1986, ApJ, 306, L109

Hurwitz, M., Sasseen, T. P., & Sirk, M. M. 2005, ApJ, in press

Innes, D. E., & Hartquist, T. W. 1984, MNRAS, 209, 7

Inoue, H., Koyama, K., Matsuoka, M., Ohashi, T., Tanaka, Y., & Tsunemi, H. 1979, ApJ, 227, L85

Jenkins, E. 1978, ApJ, 219, 845

Kaastra, J. S., & Jansen, F. A. 1993, A&AS, 97, 873

Kharchenko, V., & Dalgarno, A. 2001, ApJ, 554, L99

Kuntz, K. D., & Snowden, S. L. 2000, ApJ, 543, 195

Kuntz, K. D., Snowden, S. L., & Verter, F. 1997, ApJ, 484, 245

Lallement, R. 2004, A&A, 418, 143

Lallement, R., & Bertin, P. 1992, A&A, 266, 479

Lallement, R., Welsh, B. Y., Vergely, J. L., Crifo, F., & Sfeir, D. 2003, A&A, 411, 447

Luhman, K. L. 2001, ApJ, 560, 287

Lumb, D. H., Warwick, R. S., Page, M., & De Luca, A. 2002, A&A, 389, 93

Markevitch, M., et al. 2003, ApJ, 583, 70

McCammon, D., & Sanders W. T. 1990, ARA&A, 28, 657

McCammon, D., et al. 2002, ApJ, 576, 188

Oegerle, W. R., Jenkins, E. B., Shelton, R. L., Bowen, D. V., & Chayer, P. 2005, ApJ, in press

Poletto, G., Suess, S. T., Bemporad, A., Schwadron, N., Elliott, H., Zurbuchen, T., & Ko, Y.-K. 2004, ApJ, 613, L173

Reynolds, R. J. 1990, ApJ, 348, 153

Rocchia, R., Arnaud, M., Blondel, C., Cheron, C., Christy, J. C., Rothenflug, R., Schnopper, H. W., & Delvaille, J. P. 1984, A&A, 130, 53

Romanik, C. J. 1988, ApJ, 330, 1022

Romanik, K. 1996, Ph.D. thesis, Univ. California, Berkeley

Sanders, W. T., Edgar, R. J., Kraushaar, W. L., McCammon, D., & Morgenthaler, J. P. 2001, ApJ, 554, 694

Sanders, W. T., Kraushaar, W. L., Nousek, J. A., & Fried, P. M. 1977, ApJ, 217, L87

Schnopper, H. W., et al. 1982, ApJ, 253, 131

Seward, F. D. 2000, in Allen's Astrophysical Quantities, ed. D. P. Cox (4th ed.; New York: AIP), 197

Shelton, R. L. 2003, ApJ, 589, 261

Shelton, R. L., & Cox, D. P. 1994, ApJ, 434, 599

Smith, R. K., Brickhouse, N. S., Liedahl, D. A., & Raymond, J. C. 2001, ApJ, 556, L91

Smith, R. K., & Cox, D. P. 2001, ApJS, 134, 283

Snowden, S. L., Collier, M. R., & Kuntz, K. D. 2004, ApJ, 610, 1182

Snowden, S. L., Cox, D. P., McCammon, D., & Sanders, W. T. 1990, ApJ, 354, 211

Snowden, S. L., Freyberg, M. J., Kuntz, K. D., & Sanders, W. T. 2000, ApJS, 128, 171

Snowden, S. L., McCammon, D., & Verter, F. 1993, ApJ, 409, L21

Tanaka, Y., & Bleeker, J. A. M. 1977, Space Sci. Rev., 20, 815

Vedder, P. W., Canizares, C. R., Markert, T. H., & Pradhan, A. K. 1986, ApJ, 307, 269

Verner, D. A., & Ferland, G. J. 1996, ApJS, 103, 467

Wargelin, B. J., Markevitch, M., Juda, M., Kharchenko, V., Edgar, R. J., & Dalgarno, A. 2004, ApJ, 607, 596

Webb, D. F. 2002, in Proc. SOHO-11 Symp., From Solar Min to Max: Half a Solar Cycle with SOHO, ed. A. Wilson (ESA SP-508; Noordwijk: ESA), 409

Welsh, B. Y., Vedder, P. W., & Vallerga, J. V. 1990, ApJ, 358, 473

Welsh, B. Y., Vedder, P. W., Vallerga, J. V., & Craig, N. 1991, ApJ, 373, 556

Williamson, F. O., Sanders, W. T., Kraushaar, W. L., McCammon, D., Borken, R., & Bunner, A. N. 1974, ApJ, 193, L133